Searches for invisibly decaying Higgs bosons with the CMS detector

Patrick James Dunne
of Imperial College London

A dissertation submitted to Imperial College London
for the degree of Doctor of Philosophy

Abstract

Declaration

This dissertation is the result of my own work, except where explicit reference is made to the work of others, and has not been submitted for another qualification to this or any other university. This dissertation does not exceed the word limit for the respective Degree Committee.

Patrick Dunne

Acknowledgements

Contents

Contents

Chapter 1

Introduction and theory

This chapter will explain the theory of invisible decays of the Higgs boson ("Higgs to invisible"). It will start with an introduction to the standard model (SM), focussing on the Higgs mechanism, before outlining the motivations behind and some candidates for physics beyond the SM (BSM). Natural units, where $\hbar = c = 1$, Einstein summation convention and Feynman slash notation are used throughout. Four vector indices are labelled using greek letters, and gauge group generators using roman letters.

1.1 The standard model of particle physics

The SM describes the interaction of the particles currently thought to be fundamental with the strong, weak and electromagnetic forces. Its predictions, which come from specifying the symmetries the theory respects and how they are broken, the particles in the theory, and 18 free parameters, have been tested in many different experiments, in some cases up to one part in a trillion [1]. However, it does face challenges, described in section Section 1.2.3, one example being that it does not describe dark matter.

The SM is a gauge invariant quantum field theory (QFT). To construct a QFT the symmetries that are respected by the theory and the fields it describes must be specified. The symmetries are important because of Noether's theorem, which states that for every continuously differentiable symmetry of the Lagrangian of a theory there is a corresponding conservation law [2,3]. An example of this is Poincaré invariance, the invariance of the laws of physics under translations and rotations in space and time, which leads through Noether's theorem to the conservation of energy, linear momentum and angular momentum. In addition to giving rise to conservation laws, some types of

Table 1.1: The fundamental fermions observed in nature separated into their three generations. Each particle shown also has an antiparticle with opposite charge and identical mass. Values taken from [5]

Generation	Leptons			Hadrons		
	Particle	Mass	Charge	Particle	Mass	Charge
1	e^-	511 keV	-1	u	2.3 MeV	$+\frac{2}{3}$
	ν_e	~ 0	0	d	4.8 MeV	$-\frac{1}{3}$
2	μ^-	105.7 MeV	-1	c	1.275 GeV	$+\frac{2}{3}$
	ν_μ	~ 0	0	s	95 MeV	$-\frac{1}{3}$
2	τ^-	1.777 GeV	-1	t	173.2 GeV	$+\frac{2}{3}$
	ν_τ	~ 0	0	b	4.18 GeV	$-\frac{1}{3}$

symmetry lead to additional fields being required to preserve invariance, this will be discussed further in Section 1.1.2 [4].

It is important to specify the fields described by the QFT as these are constrained by the fundamental particles seen in nature. This is because particles correspond to the quantised excitations of fields. Specifically, scalar fields correspond to spin zero bosons, spinor fields correspond to spin half fermions, and vector fields correspond to spin 1 bosons. In order to add a new field an explanation for why the corresponding particle has not yet been observed must, therefore, be provided. We will now go through the particles observed in nature and how they are represented in the SM.

1.1.1 Fundamental particles in nature

There are two types of fundamental particles in nature, fermions and bosons. The fermions observed in nature that are currently thought to be fundamental are then divided into those which interact via the strong nuclear force (the quarks), and those which don't (the leptons). Both the quarks and leptons have two further types: charged and neutral in the case of the leptons, and up type and down type in the case of the fermions. Another interesting feature of the fermions is that they are arranged in three generations. Each generation has one fermion of each type with the same quantum numbers as those in the other generations, except that the mass is different. Table 1.1 shows this structure.

Table 1.2: The fundamental vector bosons observed in nature separated by the force which they mediate. Values taken from [5].

Force	Particle	Mass	Charge
Electromagnetism	γ	0	0
Weak	$W^{\pm}$	80.4 GeV	± 1
	Z	91.2 GeV	0
Strong	g	0	0

The bosons in nature also have two types. The first type are vector bosons which mediate the three fundamental interactions described by the SM. The vector bosons are summarised in Table 1.2, where it can be seen that their masses are very different, the photon and the eight gluons being massless, while the $W^{\pm}$ and Z bosons are very massive. As we will see in Section 1.2.1 explaining these masses requires the Higgs mechanism. The Higgs mechanism also gives rise to the other type of boson seen in nature, the scalar Higgs boson. In order to see how all of the above particles are represented in the SM an introduction to gauge theories is necessary.

1.1.2 Introduction to gauge theories

Gauge symmetries are local transformations, i.e. the transformation can be different at different points in space and time, that form a symmetry group. To see the effect of imposing such a symmetry on a theory consider imposing local invariance under U(1) transformations on the Dirac Lagrangian for a masssive fermion:

$$\mathcal{L} = i\bar{\psi}\displaystyle{\not}\partial\psi - m\bar{\psi}\psi \; [6].$$

(1.1)

This Lagrangian is invariant under a global $U(1)$ transformation $\psi \to e^{iq\theta}\psi$, where q and θ are constant. However, if the $U(1)$ transformation is local i.e. θ is a function of spacetime position the Lagrangian is no longer invariant and transforms as:

$$\mathcal{L} \to \mathcal{L} - q(\partial_{\mu}\theta)\bar{\psi}\gamma^{\mu}\psi.$$

(1.2)

In order to restore invariance a vector field, A_μ, referred to as a gauge field or gauge boson, which transforms as $A_\mu \to A_\mu + \partial_\mu\theta$ and has an interaction with the fermion field:

$$\mathcal{L}_{int} = q(\bar{\psi}\gamma^\mu\psi)A_\mu, \tag{1.3}$$

can be added to the theory. The interaction term of the new gauge field transforms as:

$$\mathcal{L}_{int} \to \mathcal{L}_{int} + q(\partial_\mu\theta)\bar{\psi}\gamma^\mu\psi, \tag{1.4}$$

which cancels out the non-gauge invariance seen in equation (1.2).

Assuming the new gauge field to be massless the Lagrangian is now:

$$\mathcal{L} = i\bar{\psi}\slashed{\partial}\psi - m\bar{\psi}\psi + q(\bar{\psi}\gamma^\mu\psi)A_\mu - \frac{1}{4}F_{\mu\nu}F^{\mu\nu}, \tag{1.5}$$

where $F_{\mu\nu}$ is the field strength tensor of the vector field. For a gauge boson from a general gauge group is written as:

$$F_{\mu\nu}^a = \partial_\mu A_\nu^a - \partial_\nu A_\mu^a + gfabcA_\mu^b A_\nu^c, \tag{1.6}$$

where f^{abc} are the structure constants of the gauge group, which are a representation of the comutation relations between the group's generators. For $U(1)$ which only has one self-commuting generator the single structure constant is 0. However, for non-Abelian gauge groups (i.e. those with non-commuting generators) they can be non-zero causing the $F_{\mu\nu}F^{\mu\nu}$ term in the Lagrangian to include self-interaction terms of the vector bosons.

It is also interesting to note that equation (1.5) can be rewritten as:

$$\mathcal{L} = i\bar{\psi}\gamma^\mu\mathcal{D}_\mu\psi - m\bar{\psi}\psi - \frac{1}{4}F_{\mu\nu}F^{\mu\nu}, \tag{1.7}$$

where $\mathcal{D}_\mu = \partial_\mu + iqA_\mu$ and is referred to as the covariant derivative. Comparing equation (1.1) and equation (1.7) it can be seen that to go from a globally invariant Lagrangian to a locally invariant one we have substituted the normal spacetime derivative for the covariant derivative and added the free term of the vector field.

$U(1)$ transformations have one degree of freedom and can be described by one parameter, in the above case θ, and in order to make the Lagrangian locally invariant one interacting gauge boson had to be added. This correspondence between the number of degrees of freedom and the number of gauge bosons holds generally. For each degree of freedom of

a group's transformations there exists a generator of the group, and for each generator one interacting gauge boson must be added to achieve local invariance.

1.2 The SM gauge group and fundamental particle representations

The SM is gauge invariant under the group $SU(3)_C \otimes SU(2)_L \otimes U(1)_Y$. Fermions in the SM are spin half spinor representations of these symmetry groups. These spinors can be split into chirally left and right handed components using the projection operators $P_{L \atop R} = \frac{1}{2}(1 \mp \gamma^5)$. Chirally left and right handed fermions transform differently under $SU(2)_L$. The right handed spinors are not charged under $SU(2)_L$ and thus are represented as a singlet, while the left handed spinors transform as a doublet.

The first generation of leptons can, therefore, be written as:

$$\psi_1 = e_R, \; \psi_2 = L = \begin{pmatrix} \nu_e \\ e_L \end{pmatrix}. \tag{1.8}$$

The SM treats neutrinos as massless and has no right handed neutrino. Similarly the first generation of quarks can be written as:

$$\psi_3 = u_R, \; \psi_4 = d_R, \; \psi_5 = \begin{pmatrix} u_L \\ d_L \end{pmatrix}. \tag{1.9}$$

As we saw in Section 1.1.2 gauge symmetries in theories with fermions require the addition of an interacting vector boson per symmetry generator to preserve gauge invariance. $SU(3)_C$ has eight generators whose eight vector bosons, $G_{a\mu}$, correspond to the eight physical gluons which mediate the strong interaction. $SU(2)_L$ has three generators whose three vector bosons, W_μ^i, mix with the one vector boson from $U(1)_Y$, B_μ unifying the electromagnetic and weak forces into one electroweak force. The physical states that

result are:

$$W^{\pm}{}_{\mu} = \frac{1}{\sqrt{2}} \left(W^1_{\mu} \mp i W^2_{\mu} \right)$$
$$Z_{\mu} = cos\left(\theta_W\right) W^3_{\mu} - sin\left(\theta_W\right) B_{\mu} \tag{1.10}$$
$$A_{\mu} = sin\left(\theta_W\right) W^3_{\mu} + cos\left(\theta_W\right) B_{\mu},$$

where θ_W is the Weinberg angle and A_{μ} is the photon field. Also, as described in Section 1.1.2 the interaction between these vector bosons and the fermion fields occurs through their presence in the covariant derivative, and interactions between the vector bosons occur because $SU\left(3\right)_C$ and $SU\left(2\right)_L$ are non-Abelian.

Now let us try to construct a Lagrangian for these fields. First ignoring the masses we find:

$$\mathcal{L} = i\bar{\psi}_i \not{D} \psi_i - \frac{1}{4} F_{\mu\nu j} F_j^{\mu\nu}, \tag{1.11}$$

where the sum over all ψ also includes the second and third generations, $F_{\mu\nu j} F_j^{\mu\nu}$ is a sum of the free terms of all the SM gauge bosons and $\mathcal{D}$ is the SM covariant derivative:

$$\mathcal{D}_{\mu} = \partial_{\mu} + ig_1 \frac{Y}{2} B_{\mu} + ig_2 \frac{\tau_i}{2} W^i_{\mu} + ig_3 \frac{\lambda_a}{2} G^a_{\mu}, \tag{1.12}$$

with Y being the constant generator of $U\left(1\right)$, τ_i the generators of $SU\left(2\right)_L$, λ_a the generators of $SU\left(3\right)_C$ and g_i the coupling constants of the fields. It should be noted that $\frac{g_1}{g_2}$ is equal to $\tan\left(\theta_W\right)$.

When we try to include mass a problem occurs. We know that some of the fermions have mass, and consequently we should have fermion mass terms of the form:

$$\mathcal{L}_{m_f} = -m_f \bar{f} f$$
$$= -m_f \bar{f} \left[\frac{1}{2} \left(1 - \gamma^5 \right) + \frac{1}{2} \left(1 + \gamma^5 \right) \right] f \tag{1.13}$$
$$= -m_f \left(\bar{f}_R f_L + \bar{f}_L f_R \right),$$

in our Lagrangian. However, as the left and right handed fields do not transform in the same way under $SU\left(2\right)_L$ this term breaks the gauge symmetry of the Lagrangian and can't be present.

A similar problem occurs for vector fields. In Section 1.1.2 we didn't consider the mass term of these vector fields:

$$\mathcal{L}_{m_V} = \frac{1}{2} m_V^2 A_\mu A^\mu, \tag{1.14}$$

which is not gauge invariant, so massive vector bosons are not possible on their own in gauge invariant theories either. The additional piece of the SM required to allow particles to have mass is the Higgs mechanism.

1.2.1 Spontaneous symmetry breaking and the Higgs mechanism

The Higgs mechanism is a form of spontaneous symmetry breaking. A symmetry is said to be spontaneously broken when the Lagrangian remains invariant while the vacuum state, i.e. that with lowest energy, does not. Terms which are not gauge invariant can then be incorporated into the theory by adding a field which has a non-zero vacuum expectation value and coupling it to the other fields present in the term. For the Higgs mechanism this field is a complex scalar $SU(2)_L$ doublet, called the Higgs field:

$$\phi = \begin{pmatrix} \phi^+ \\ \phi^0 \end{pmatrix}. \tag{1.15}$$

The main part of the Higgs field Lagrangian is:

$$\mathcal{L} = T - V = (\mathcal{D}_\mu \phi)^\dagger (\mathcal{D}^\mu \phi) + \mu^2 \phi^\dagger \phi - \lambda \left(\phi^\dagger \phi \right)^2. \tag{1.16}$$

For $\mu^2 > 0$ the minima of the potential are non-zero and form a circle in phase space of ϕ. All of these vacua are equivalent and a particular vucuum can be chosen with no physical effect. By convention we choose the following vacuum:

$$\langle 0|\phi|0 \rangle = \begin{pmatrix} 0 \\ \sqrt{\frac{\mu^2}{2\lambda}} \end{pmatrix} = \frac{1}{\sqrt{2}} \begin{pmatrix} 0 \\ v \end{pmatrix}. \tag{1.17}$$

Next we consider small perturbations around this vacuum, ignoring those that can be set to zero by gauge freedom gives:

$$\phi = \begin{pmatrix} 0 \\ v + H \end{pmatrix}. \tag{1.18}$$

Inserting this into equation (1.16) and ignoring terms with more than one type of field gives at leading order:

$$\mathcal{L} = \frac{1}{2}\partial_\mu H \partial^\mu H - \frac{1}{2}\mu^2 H^2 + \frac{v^2}{8}\left[g_2^2 W_\mu^+ W^{+\mu} + g_2^2 W_\mu^- W^{-\mu} + \left(g_1^2 + g_2^2\right) Z_\mu Z^\mu\right]. \tag{1.19}$$

As expected, the weak vector bosons $W_\mu^\pm$ and Z_μ aquire masses $\frac{gv}{2}$ and $\frac{v}{2}\sqrt{g_1^2 + g_1^2}$ respectively. We also see an additional massive scalar H, which is the Higgs boson, which has mass $\sqrt{2}\mu$. The photon and gluons do not aquire masses as the particular choice of coupling constants and the structure of the group generators leads to the terms in A_μ and $G_{\mu a}$ being zero.

The final part of the Higgs field Lagrangian is that giving rise to the fermion masses. These are generated by a Yukawa term in the Lagrangian for each fermion as follows:

$$\mathcal{L}_{Yuk} = k_f \left(\bar{f}_L \phi f_R + \bar{f}_R \phi^\dagger f_L\right). \tag{1.20}$$

The fermion's mass is then $\frac{k_f v}{\sqrt{2}}$.

1.2.2 Higgs boson production and decay at the LHC

1.2.3 Challenges for the SM

1.3 Dark matter

1.4 Some extensions of the standard model incorporating dark matter

Chapter 2

The LHC and the CMS experiment

The purpose of this chapter is to introduce the CMS experiment [7] and the LHC [8]. Without both of these apparatus the analyses performed for this thesis would, of course, not have been possible. In Section 2.1 an overview of the LHC and the chain of accelerators which feed into it will be given. This will then be followed in Section 2.2 by a description of the CMS experiment focussing on the aspects most relevant to the search for invisibly decaying Higgs bosons.

2.1 The LHC

The LHC is situated 100m underground in a tunnel formerly built for the LEP accelerator [9] at CERN near Geneva, Switzerland. It is a 27km storage ring which accelerates both protons and heavy ions and collides them at the highest centre of mass energies of any collider built to date. The work contained in this thesis uses data from proton-proton collisions ("events"). These protons are obtained by taking hydrogen gas and stripping its atoms of their electrons with an electric field. The first accelerator in the LHC accelerator sequence, Linac 2, accelerates the protons to 50 MeV. The protons are then accelerated to 1.4 GeV by the next accelerator, the Proton Synchrotron Booster (PSB), which is followed by the Proton Synchrotron (PS) where they reach 25 GeV. The beam energy is then increased to 450 GeV in the Super Proton Synchrotron (SPS). Finally, the protons are injected into the LHC where, at time of writing, the maximum energy the beams have been accelerated to is 6.5 TeV, close to the design maximum of 7 TeV.

When fully filled the LHC contains two counter-rotating beams which are formed of up to 2808 bunches spaced either 25 or 50 ns apart and each containing $\mathcal{O}(10^{11})$ protons.
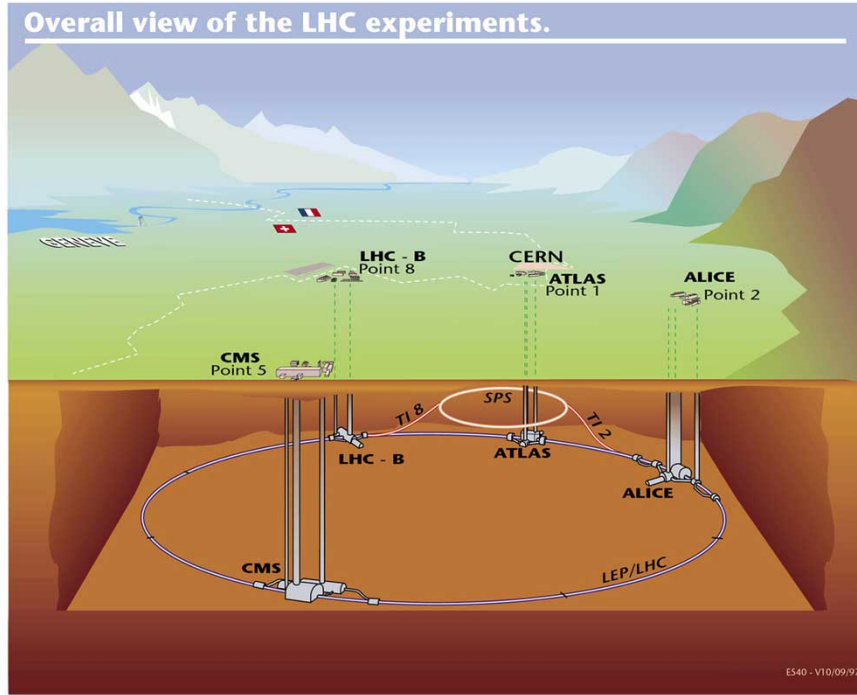
Figure 2.1: The layout of the LHC accelerator chain, showing the position of the four main detectors.

The two beams are kept travelling in a cirlce by 1232 superconducting dipole magnets and steered to four collision points around the LHC. Detectors are situated at these collision points to observe the collisions, the main four being: ALICE [10], ATLAS [11], CMS [7] and LHCb [12]. A schematic of the LHC accelerator chain and the detectors can be seen in Figure 2.1.

When studying a physical process occuring in particle collisions it is important to know how many times it will occur, this can be expressed as:

$$N = \mathcal{L}\sigma, \tag{2.1}$$

where $\mathcal{L}$, the integrated luminosity, depends only on the parameters of the collisions, and the cross-section depends only on the process. In order to observe rare (i.e. low cross-section) processes, such as those studied at the LHC, it is, necessary to use very high luminosity datasets. The integrated luminosity is obtained by integrating the instantaneous luminosity over time, so large luminosities can be obtained either by running the accelerator for a long time, or by operating at high instantaneous luminosity.

For collisions at the LHC the instantaneous luminosity is given by:

$$\mathcal{L} = \frac{k_b N_b^2 f_{rev} \gamma}{4\pi \epsilon_n \beta}[13],\tag{2.2}$$

where k_b is the number of bunches per beam, N_b the number of protons per bunch, f_{rev} the revolution frequency, ϵ_n the normalised transverse beam emittance, β^* the beta-function at the interaction point and γ the Lorentz factor. The design instantaneous luminosity of the LHC is $10^{34}\,\mathrm{cm}^{-2}\mathrm{s}^{-1}$ with 25ns bunch spacing.

The LHC started physics runs in 2010, during which it operated at a centre of mass energy of 7 TeV and delivered an integrated luminosity of 44.2 pb^{-1} to CMS. In 2011 the LHC also operated at 7 TeV and delivered 6.1fb^{-1} to CMS. The centre of mass energy was increased to 8 TeV in 2012 and 23.3fb^{-1} of data were delivered to CMS. A summary of the luminosity delivered to CMS during the three periods of run 1 can be seen in Figure 2.2. In run 2 the centre of mass energy was further increased to 13 TeV and during 2015 4.09fb^{-1} of data were delivered to CMS at this energy. In order to be used for physics analysis data must be certified. This certification ensures that the detector was fully operational when the data were recorded. In 2011 5.1fb^{-1} were certified, in 2012 19.7fb^{-1} were certified and in 2015 2.2fb^{-1} were certified.

The cross-section for several processes is shown in Figure 2.3 and it can be seen that the cross-section for VBF Higgs production is approximately 1.5 pb. Therefore, we expect approximately 30000 VBF produced Higgs bosons in the 2012 dataset. By contrast the vector boson production cross section is approximately 100 nb and the total cross-section for any process is orders of magnitude higher still. The separation of the relatively small number of signal events from the large background is a major challenge for the search for Higgs to invisible.

The large total cross-section combined with the high instantaneous luminosities that the LHC operates at leads to the probability for multiple proton-proton interactions per bunch crossing being high. The distribution of the number of interactions per bunch crossing can be seen in Figure 2.4. The additional interactions on top of the process of interest in a bunch crossing are called pile-up pile-up (PU).
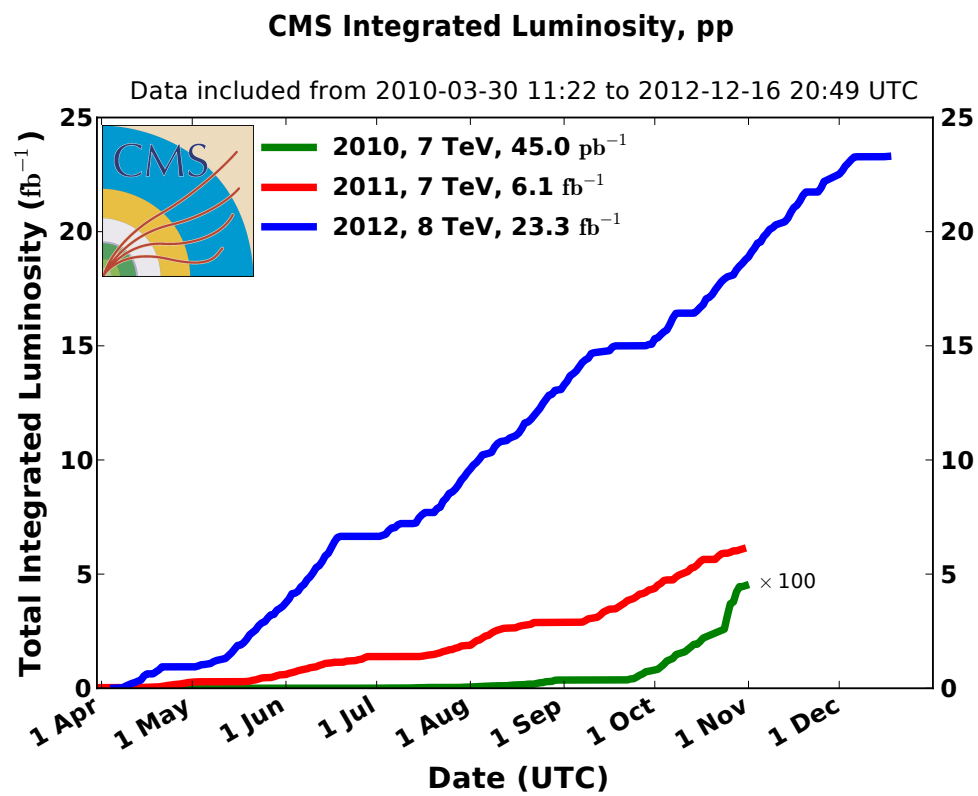
Figure 2.2: A summary of the luminosity delivered to CMS during Run 1 of the LHC [14].
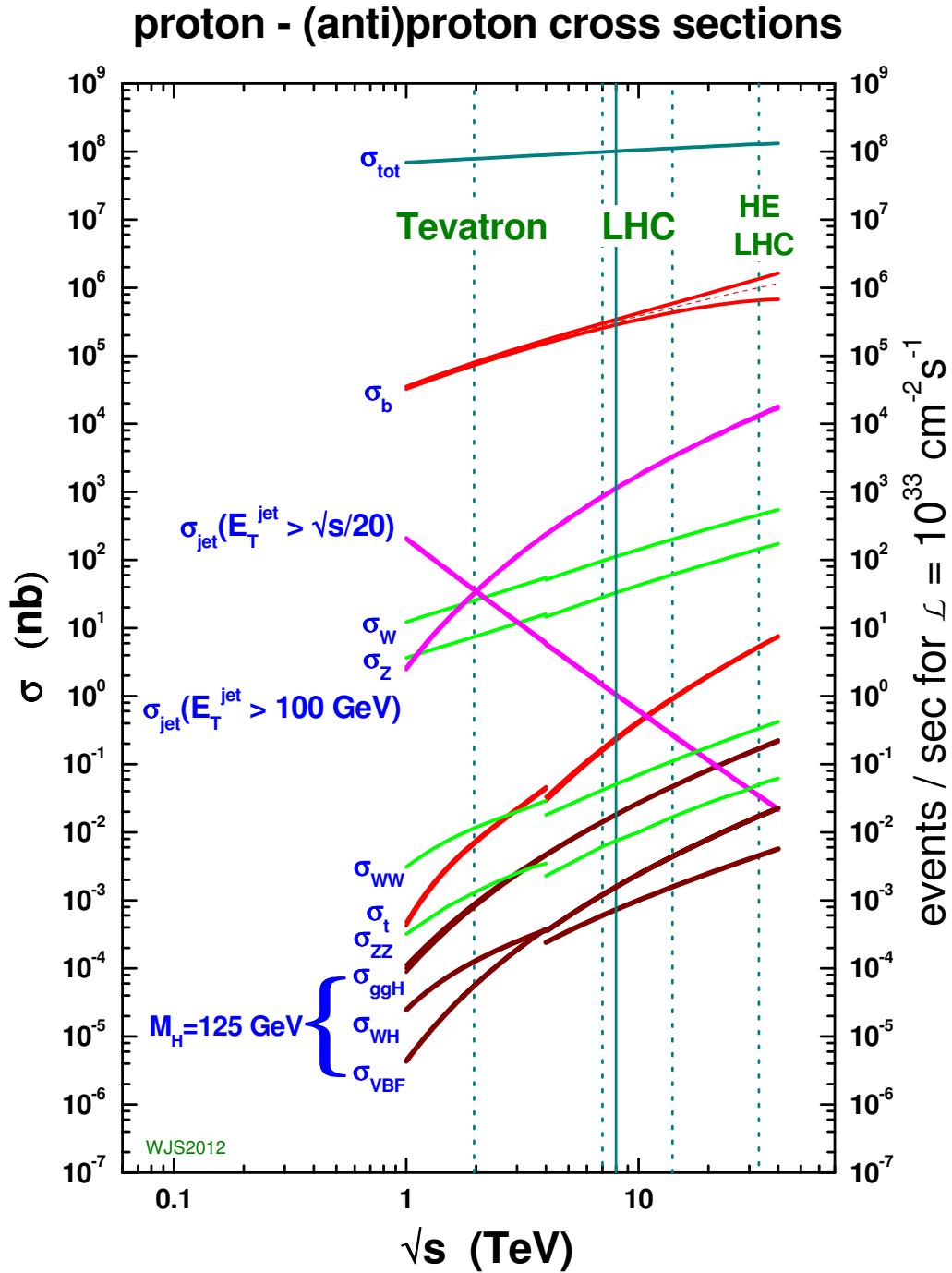
Figure 2.3: Cross sections for several processes in collisions of protons with protons or anti-protons as a function of centre of mass energy. The energies that the LHC and Tevatron ran at are highlighted [15].
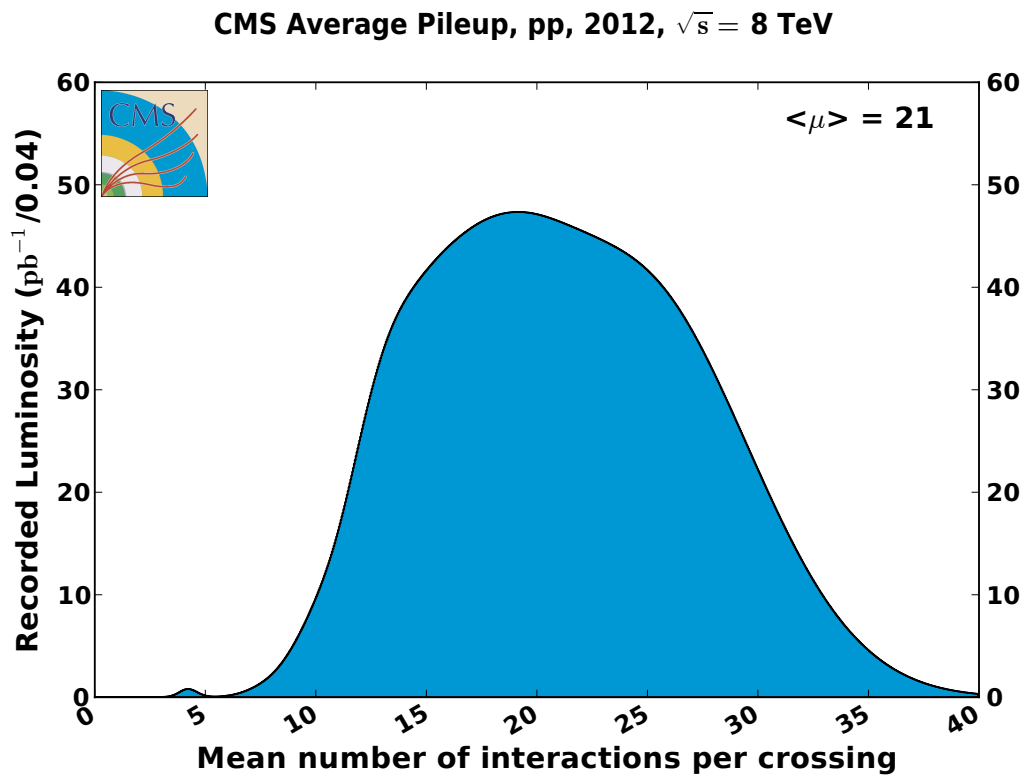
Figure 2.4: Distribution of the number of interactions per bunch crossing in CMS during 2012 running of the LHC [14].
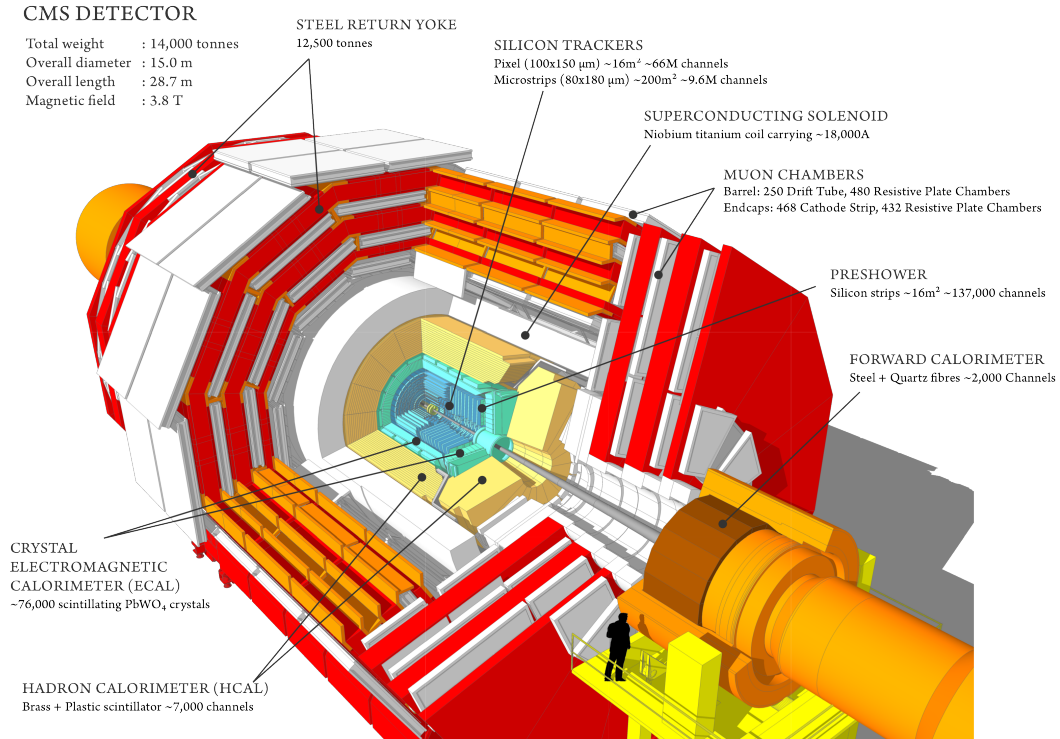
CMS DETECTOR

Total weight   : 14,000 tonnes
Overall diameter : 15.0 m
Overall length   : 28.7 m
Magnetic field   : 3.8 T

STEEL RETURN YOKE
12,500 tonnes

SILICON TRACKERS
Pixel (100x150 µm) ~16m² ~66M channels
Microstrips (80x180 µm) ~200m² ~9.6M channels

SUPERCONDUCTING SOLENOID
Niobium titanium coil carrying ~18,000A

MUON CHAMBERS
Barrel: 250 Drift Tube, 480 Resistive Plate Chambers
Endcaps: 468 Cathode Strip, 432 Resistive Plate Chambers

PRESHOWER
Silicon strips ~16m² ~137,000 channels

FORWARD CALORIMETER
Steel + Quartz fibres ~2,000 Channels

CRYSTAL
ELECTROMAGNETIC
CALORIMETER (ECAL)
~76,000 scintillating PbWO₄ crystals

HADRON CALORIMETER (HCAL)
Brass + Plastic scintillator ~7,000 channels

Figure 2.5: A diagram of the subsystems making up the CMS detector, illustrating the hermeticity and layered structure of the experiment [16].

2.2 The CMS experiment

The CMS detector was designed to search for the SM Higgs and new physics at the TeV energy scale. Both because the nature of new physics is not known and the SM Higgs has a wide range of decays and production mechanisms CMS must be sensitive to many different types of final state particles and topologies. In order to achieve this it has a hermetic design comprising a barrel, endcaps and a forward calorimetry system, and is also composed of several layers of subdetectors each sensitive to different particles as shown in Figure 2.5. The hermiticity of the detector is particularly important for the VBF Higgs to invisible search, because, as described in Section 1.2.2, the VBF final state is highly likely to have jets in the forward regions of the detector.

A central design feature of CMS is the superconducting magnet, inside which is generated a 3.8T axial field. This field bends the path of charged particles travelling through it allowing their momentum to be measured. Not all particles are charged however, and the path of several types of particles through the CMS detector is shown in Figure 2.6. The first layer is the tracker which records the paths taken by charged particles, as well as providing a momentum measurement the tracks also allow the vertex the particle came
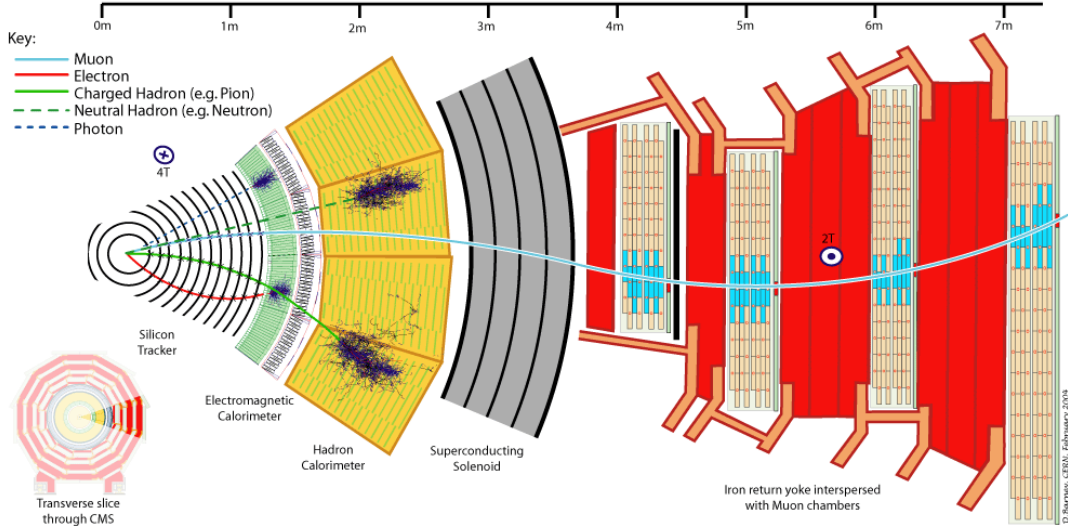
Figure 2.6: A schematic cross-section of the CMS experiment showing the path taken by several types of particles [17].

from to be identified. The next layer is the electromagnetic calorimeter (ECAL) where electrons and photons deposit energy through electromagnetic showers. This is followed by the hadron calorimeter (HCAL) where hadronic showers deposit most of their energy. After the calorimetry systems is the superconducting magnet which is not instrumented. Outside the magnet are the muon detection systems, which are interspersed with iron plates which form the return yoke for the magnet. Muons do not deposit much energy in the detector and often are not stopped, so the muon system is primarily a tracking detector.

The origin of the co-ordinate system used by CMS is at the nominal interaction point. It is a right handed cartesian system with the x axis pointing towards the centre of the LHC ring and the y-axis vertically upwards, the z axis then points along the beam line. The azimuthal angle ϕ and the polar angle θ are measured from the x and z axes respectively. It is common to describe the direction of outgoing particles using ϕ and their pseudo-rapidity, η which is defined as:

$$\eta = -\ln[\tan(\theta/2)]. \tag{2.3}$$

Distances in the $\eta - \phi$ plane are given by $\Delta R = \sqrt{\Delta\phi^2 + \Delta\eta^2}$. Two other important quantities in hadron colliders are the projections of a particle's momentum and energy in the transverse plane, these are denoted p_T and E_T respectively.
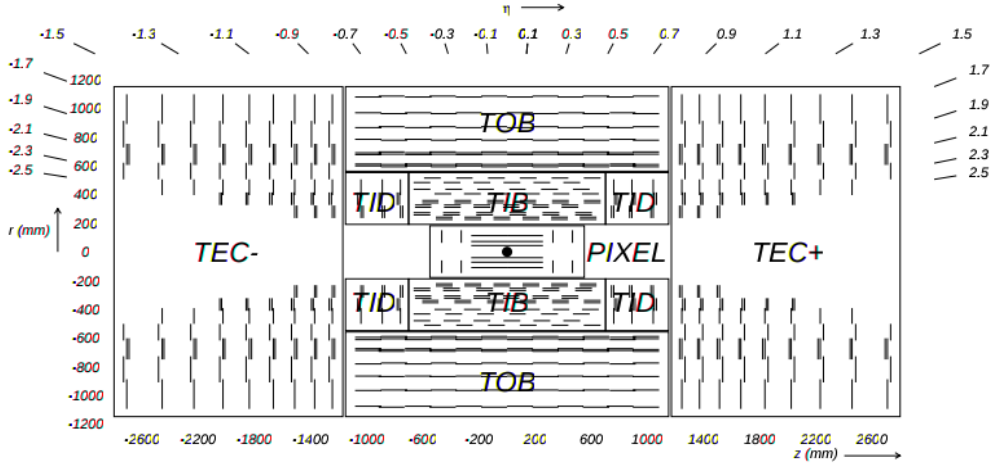
Figure 2.7: A cross-section of the CMS tracker, indicating the subsystems that comprise it. Each line indicates a detector module [7].

2.2.1 Tracker

The tracker is designed to precisely measure the paths of charged particles from LHC collisions which curve in CMS's magnetic field [7]. The design transverse momentum resolution of the full tracker detector is 1-2% at 100GeV . In order to precisely measure the particles' positions and ensure the occupance of the tracker is low a high granularity is required. Due to the frequency of collsions at the LHC and the high instantaneous luminosity a radiation hard system with fast response is also necessary. This combination of requirements motivates the use of a silicon based system. When traversing silicon charged particles create electron-hole pairs, which are then separated by an applied electric field, causing a current pulse.

The tracker layout can be seen in Figure 2.7. In order to keep the sensor occupancy below 1% at design luminosity, the innermost component is a silicon pixel detector. This detector has three layers in the barrel, at radii of 4.7, 7.3 and 10.2 cm, and two in the endcap. Each pixel is 100µmx 150µmin size and in total there are 66 million of them. The resulting resolution of the pixel detector is approximately 10µmin the $r - \phi$ plane and 17µmin the $r - z$ plane [18].

Surrounding the pixel detector is a silicon strip detector with 10 layers in the barrel, at radii of 20 to 116 cm, and 12 pairs of disks in the endcap. The strips are typically 10-20 cm long and 80-180µmwide, with the strip size increasing with radius as the particle flux decreases. The strip detector's single point resolution is 230-530µmin the $r - z$ plane

and 23-52µmin the $r - \phi$ plane. The higher resolution in the $r - \phi$ plane allows a better measurement of p_T, as this is the direction in which the particle's tracks bend in the CMS magnetic field. The barrel and endcap detectors together have an acceptance of $|\eta| < 2.5$ for both the pixel and strip detectors.

2.2.2 Electromagnetic calorimeter

The ECAL is designed to provide accurate photon and electron reconstruction and precise measurement of the electromagnetic component of hadron jets [7]. It is a homogeneous calorimeter made of lead tungstate ($PbWO_4$) crystals, separated into a barrel (ECAL barrel (EB)) section, with 61200 crystals and two endcaps (ECAL endcap (EE)) each with 7234 crystals. These crystals are 25.8 radiation lengths in depth and instrumented with photodectors, avalanche photodiodes being used in the barrel and vacuum phototriodes in the endcap.

The layout of the ECAL is shown in Figure 2.9. The EB crystals have a 170x360 arrangement in $\eta - \phi$ space such that the gaps between crystals are offset by 3° from the vector to the detector origin, thus avoiding particles travelling through the gaps. The EB extends to $|\eta| = 1.479$, with higher values of η covered by the EE. The crystals in the EE are arranged in an $x - y$ grid pointing at a focus 1.3m from the nominal interaction point, giving a $2 - 8°$ separation between the gaps between crystals and the vector to the detector origin. In addition to the main $PbWO_4$ detector the endcaps also have a preshower detector. This preshower is a lead silicon strip sampling calorimeter, which initiates the electromagnetic showers and provides sufficient position resolution to distinguish single photons from pairs produced in neutral pion decays. The total acceptance of the barrel and endcap detectors is $|\eta| < 3.0$.

On entering the ECAL high energy electrons or photons initiate an electromagnetic shower by undergoing Bremsstrahlung or pair production respectively. The resulting cascade of particles continues to lose energy by successive Bremsstrahlung and pair production until their energy is low enough that the photons no longer undergo pair-production and the electrons lose their energy mainly by ionisation. The ionisation of the $PbWO_4$ crystals leads to the emission of scintillation light, proportional to the amount of energy deposited, which is collected by the photodetectors.

The choice of $PbWO_4$ is motivated by its high density (8.28 g/cm^3), short radiation length (0.89 cm) and small Moliére radius (2.2cm), this leads to the showers being contained in
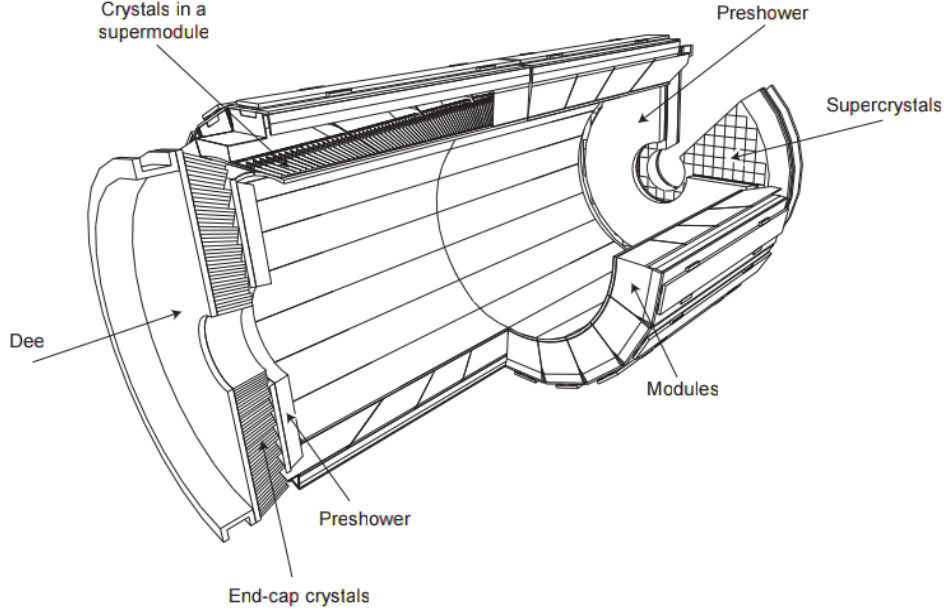
Figure 2.8: A schematic of the CMS ECAL, indicating the subsystems that comprise it [7].

a small area and allows the calorimeter to be compact and have fine granularity. Another advantage of PbWO$_4$ is that 80% of the scintillation light is emitted within the LHC's 25ns design bunch crossing time, so particles can be properly associated with the bunch crossing they originate from.

For particle energies below 500 GeV, where the resulting shower ceases to be contained in the full depth of the ECAL, the ECAL resolution can be parametrised as:

$$\left(\frac{\sigma}{E}\right)^2 = \left(\frac{S}{\sqrt{E}}\right)^2 + \left(\frac{N}{E}\right)^2 + C^2. \tag{2.4}$$

Where S is the stochastic term, N the noise term and C the constant term. The stochastic term is comprised of fluctuations in the lateral containment of showers and also in the amount of scintillation light. The noise term is made up of electronic and digital noise, and signals from other bunch crossings which do not fully dissipate in time. The constant term comes from non-uniformity of light collection along the crystals, errors in the calibration of crystals against each other and leakage of energy from the back of the calormiter. The energy resolution was measured without an applied magnetic field in an electron beam using particles with momenta between 20 and 250 GeV. The stochastic, noise and constant terms were found to be 0.028 GeV$^{1/2}$, 0.12 GeVand 0.003 respectively.
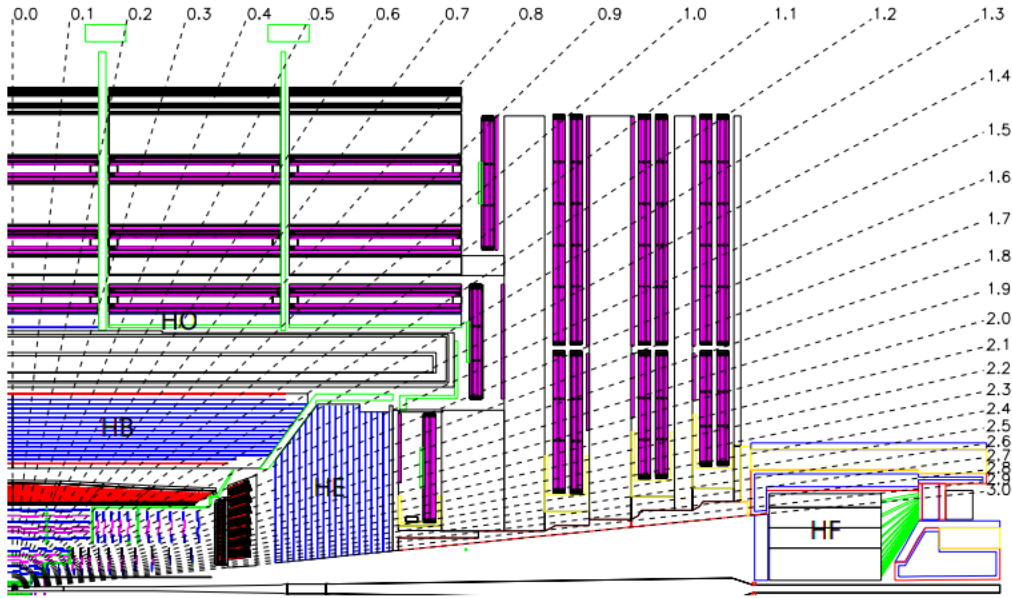
Figure 2.9: A schematic of a quadrant of the CMS HCAL in the $r - z$ plane, indicating the subsystems that comprise it [7].

2.2.3 Hadronic calorimeter

The HCAL is designed to measure the energy of strongly interacting particles. It consists of a brass and scintillator plus wavelength shifting fibre sampling calorimeter split into a barrel (hadron barrel (HB)) and endcap (hadron endcaps (HE)) section, and a radiation hard steel and quartz fibre Cherenkov forward calorimeter (hadron forward (HF)). The primary design consideration for the HCAL is that it must fit between the outer edge of the ECAL ($r = 1.77$ m) and the inner edge of the magnet ($r = 2.95$ m). In order to satisfy this requirement and achieve satisfactory containment of hadronic showers the magnet coil is also used as an absorber, and there is a further layer of scintillator outside the magnet coil (hadron outer (HO)). In total the HCAL corresponds to 10-15 interaction legnths, depending on η.

2.2.4 Muon system

2.2.5 Trigger system

Chapter 3

Physics objects and event reconstruction

3.1 Primary vertex

3.2 Jets

3.3 Missing transverse energy

3.4 Electrons

3.5 Muons

3.6 Taus

3.7 Photons

Chapter 4

Methods for limit setting

Chapter 5

Search for invisibly decaying Higgs bosons in run I prompt data

5.1 Trigger and event selection

5.2 Background estimation

5.2.1 W$\to e\nu$+jets

5.2.2 W$\to \mu\nu$+jets

5.2.3 W$\to \tau\nu$+jets

5.2.4 Z$\to \nu\nu$+jets

5.2.5 QCD

5.2.6 Minor backgrounds

5.3 Systematic uncertainties

5.4 Results

Chapter 6

Search for invisibly decaying Higgs bosons in run I parked data

6.1 Trigger

6.2 Event selection

6.3 Background estimation

6.3.1 W$\rightarrow e\nu$+jets

6.3.2 W$\rightarrow \mu\nu$+jets

6.3.3 W$\rightarrow \tau\nu$+jets

6.3.4 Z$\rightarrow \nu\nu$+jets

6.3.5 QCD

6.3.6 Minor backgrounds

6.4 Systematic uncertainties

6.5 Results

Chapter 7

Combinations and interpretations of run I searches for invisibly decaying Higgs bosons

7.1 Searches in other channels

7.2 Combination with prompt VBF search

7.3 Combination with the parked VBF search

7.4 Dark matter interpretations

Chapter 8

Search for invisibly decaying Higgs bosons in run II data

Bibliography

[1] D. Hanneke, S. Fogwell, and G. Gabrielse, "New Measurement of the Electron Magnetic Moment and the Fine Structure Constant", *Phys. Rev. Lett.* **100** (Mar, 2008) 120801, `doi:10.1103/PhysRevLett.100.120801`.

[2] E. Noether, "Invariant Variation Problems", *Gott. Nachr.* **1918** (1918) 235–257, `doi:10.1080/00411457108231446`, `arXiv:physics/0503066`. [Transp. Theory Statist. Phys.1,186(1971)].

[3] E. Noether, "Invariant variation problems", *Transport Theory and Statistical Physics* **1** (1971), no. 3, 186–207, `doi:10.1080/00411457108231446`.

[4] C. N. Yang and R. L. Mills, "Conservation of Isotopic Spin and Isotopic Gauge Invariance", *Phys. Rev.* **96** (Oct, 1954) 191–195, `doi:10.1103/PhysRev.96.191`.

[5] Particle Data Group Collaboration, "Review of Particle Physics", *Chin. Phys.* **C38** (2014) 090001, `doi:10.1088/1674-1137/38/9/090001`.

[6] D. Griffiths, "Introduction to Elementary Particles". Physics textbook. Wiley, 2008.

[7] C. Collaboration, "The CMS experiment at the CERN LHC", *JINST* **3** (2008) S08004, `doi:10.1088/1748-0221/3/08/S08004`.

[8] L. Evans and P. Bryant, "LHC Machine", *JINST* **3** (2008), no. 08, S08001, `doi:10.1088/1748-0221/3/08/S08001`.

[9] LEP Injector Study Group, "LEP design report, volume I: The LEP injector chain; LEP design report, volume II: The LEP Main Ring". CERN, Geneva, 1983.

[10] A. Collaboration, "The ALICE experiment at the CERN LHC", *JINST* **3** (2008) S08002, `doi:10.1088/1748-0221/3/08/S08002`.

[11] A. Collaboration, "The ATLAS Experiment at the CERN Large Hadron Collider", *JINST* **3** (2008) S08003, `doi:10.1088/1748-0221/3/08/S08003`.

[12] LHCb Collaboration, "The LHCb Detector at the LHC", *JINST* **3** (2008) S08005, `doi:10.1088/1748-0221/3/08/S08005`.

[13] M. Benedikt, P. Collier, V. Mertens et al., "LHC Design Report". CERN, Geneva, 2004.

[14] CMS Collaboration, "CMS Luminosity - Public Results",.

[15] W. J. Stirling, "Private communication",.

[16] T. Sakuma and T. McCauley, "Detector and Event Visualization with SketchUp at the CMS Experiment", *J. Phys.: Conf. Ser.* **513** 022032, `doi:10.1088/1742-6596/513/2/022032`.

[17] CMS Collaboration, "Interactive Slice of the CMS detector", *CMS Document 4172-v2.*

[18] Tricomi, Alessia, "Performances of the ATLAS and CMS silicon tracker", *Eur Phys J C* **33** (2004) s1023–s1025, `doi:10.1140/epjcd/s2004-03-1801-1`.

List of Figures

List of Tables

List of Acronyms

PSB Proton Synchrotron Booster

PS Proton Synchrotron

SPS Super Proton Synchrotron

PU pile-up

SM standard model

BSM beyond the SM

QFT quantum field theory

ECAL electromagnetic calorimeter

HCAL hadron calorimeter

EB ECAL barrel

EE ECAL endcap

HB hadron barrel

HE hadron endcaps

HF hadron forward

HO hadron outer